A finite element study on the cause of vocal fold vertical stiffness variation

Biao Geng, Qian Xue, and Xudong Zheng

Citation: The Journal of the Acoustical Society of America **141**, EL351 (2017); doi: 10.1121/1.4978363
View online: http://dx.doi.org/10.1121/1.4978363
View Table of Contents: http://asa.scitation.org/toc/jas/141/4
Published by the Acoustical Society of America

A finite element study on the cause of vocal fold vertical stiffness variation

Biao Geng, Qian Xue,[a] and Xudong Zheng
Department of Mechanical Engineering, University of Maine, Orono, Maine 04473, USA
biao.geng@maine.edu, qian.xue@maine.edu, xudong.zheng@maine.edu

Abstract: A finite element method based numerical indentation technique was used to quantify the effect of the material stiffness variation and the subglottal convergence angle of the vocal fold on the vertical stiffness difference of the medial surface. It was found that the vertical stiffness difference increased with the increasing subglottal angle, and it tended to saturate beyond a subglottal angle of about 50°. The material stiffness variation could be as important as the subglottal angle depending on the actual material properties.

[DDO]
Date Received: September 27, 2016 **Date Accepted:** February 21, 2017

1. Introduction

Vertical stiffness variation on the vocal fold medial surface was recently reported in both human (Chhetri *et al.*, 2011; Chhetri and Rafizadeh, 2014) and canine (Chhetri *et al.*, 2014; Oren *et al.,* 2014) samples. Using indentation, the local stiffness on the medial surface of both intact vocal folds and combined epithelium and lamina propria layers dissected and separated from the vocal fold muscle was measured. Vertical stiffness variation with the inferior aspect being significantly stiffer than the superior was observed in all the samples. This vertical stiffness variation was proposed to be important for phonation as it can promote the divergent angle during the vibration (Oren *et al.,* 2014). Beside experimental measurements, vertical stiffness variation has also been common in spring-mass vocal fold models (see, e.g., Ishizaka and Flanagan, 1972; Story and Titze, 1995; Yang *et al.*, 2010; Yang *et al.*, 2012). Yang *et al.* (2012) showed that it is essential to have this feature in order for the spring-mass models to match *in vivo* vocal fold kinematics. They suggested that these results support the proposition by Goodyer *et al.* (2010) that the vertical stiffness variation may provide a more efficient transfer of energy across the air/tissue boundary. The potential beneficial effect of vertical stiffness variation on increasing divergent angle and energy transfer also gained support from a recent numerical study (Geng *et al.,* 2016) which showed that increasing the vertical stiffness variation would increase the peak flow rate, divergent angle and sound intensity during vibration.

While the importance of the vertical stiffness variation is attracting more attention, the mechanism of such feature has not been studied. Chhetri *et al.* (2011) proposed that the variation of the stiffness was in accordance with the material variation from the subglottic cricothyroid membrane to the lamina propria about half way along the medial surface in the vertical direction. However, it should be noticed that the stiffness obtained by micro indentation is derived from the slope of the force-displacement curve. It represents the local contact stiffness which is generally a function of many properties including the material properties, material orientation, geometric dimensions, loading direction, and type of constraint. Therefore, in the measurement of the intact vocal fold samples, in addition to the material property (i.e., elastic moduli) variation, the subglottal convergence angle of the vocal fold (Xu *et al.*, 2017, hereafter referred to as the subglottal angle) can also contribute to the stiffness variation. Nevertheless, measurement on the intact vocal fold best resembles the scenario where the glottal flow interacts with the vocal fold, thus the results would provide useful information for understanding the dynamics. It remains unclear how the subglottal angle and material variation interact to affect the total stiffness variation. Furthermore, Oren *et al.* (2014) suggested that proximity to the conus elasticus might be another mechanism causing the inferior aspect to be stiffer. However, the proposition was not verified.

[a]Author to whom correspondence should be addressed.

This study aims to use the finite element method to quantify the contribution of the first two mechanisms (the material variation and the nonzero subglottal angle) to the vertical stiffness variation of the vocal fold. The modelling of the conus elasticus is not feasible for the time being since there are little quantified data about its structure. Furthermore, as the fibers of the conus elasticus run from the cricoid cartilage to the ligament (Reidenbach, 1996), its plane of isotropy is different from that of the other layers and generally varies along the fiber.

The findings of this study have important implication to vocal fold treatment and modeling as it points out how to effectively restore and model the stiffness variation in vocal fold. In the study, the subglottal angle of the vocal fold models was varied in a large range, and the material variation was modeled by varying the elastic moduli (material stiffness) of the cover layer tissue. The numerical indentation method, which was based on an in-house finite element solver, was first verified against the analytical solution and then used to investigate the effect of the subglottal angle and combined effects of the subglottal angle and material variation on the total vertical stiffness variation.

2. Methods

2.1 Numerical indentation and its verification

In the current study, a numerical indentation method based on the linear elasticity theory was employed to measure the local stiffness on the vocal fold medial surface. Figure 1(a) shows the schematic of an infinite half-space subjected to a circular uniform normal load on the boundary. For an isotropic material, the analytical solution to this problem can be readily found in elasticity textbooks. The maximum normal displacement takes place at the center of the circle and can be calculated as

$$\Delta x_{\max} = \frac{2(1-\mu^2)pR}{E}, \tag{1}$$

where $\Delta x_{\max}$ is the normal displacement at the center of the circle, μ and E are the Poisson's ratio and Young's modulus of the material, respectively, p is the applied pressure, and R is the radius of the circle. It can be derived from Eq. (1) that

$$\frac{pR}{\Delta x_{\max}} = \frac{E}{2(1-\mu^2)}. \tag{2}$$

On the left-hand side of Eq. (2), pR can be seen as a measurement of the loading force and $\Delta x_{\max}$ is a measurement of the yielding of the indented object. Thus $pR/\Delta x_{\max}$ can be used as a measurement of the local stiffness at the indentation point regardless of the material type, it has the unit of elastic moduli. For the aforementioned half-space problem, the stiffness only depends on the material properties as shown in Eq. (2). However, other factors such as geometry and constraints of the structure would also affect the stiffness if the condition of an infinite half-space is not satisfied.

The indentation was numerically implemented by solving the deformation with an in-house finite element solver. Once the deformation is solved, the local stiffness can be evaluated as

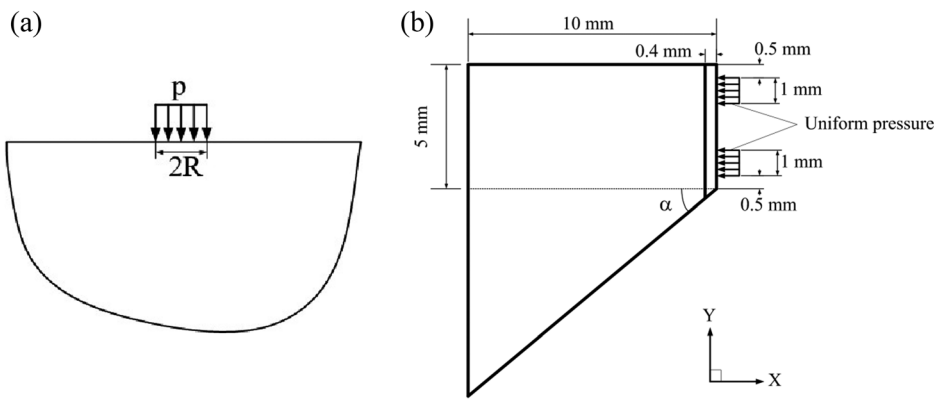

Fig. 1. (a) Schematic of the half-space problem. (b) Vocal fold profile.

$$k = \frac{pR}{\Delta x_{\max}}. \tag{3}$$

The method was verified against the theoretical solution of the aforementioned half-space problem [Eq. (2)]. Finite element simulation was performed on a 1-in. cube of isotropic material. The Young's modulus of the model was 3.14 kPa. The indenter boundary was 5.5 mm in diameter and was placed at the center of the top surface of the cube, similar to the protocol used by Chhetri *et al.* (2011). Even though the condition of an infinite half-space was not strictly satisfied, the cube was sufficiently larger than the indenter. Since the linear elasticity formulation was used, the $p - \Delta x_{\max}$ curve would be a straight line and the slope can be calculated using any of the data points. The stiffness from the numerical indentation was 1.757 kPa, which was very close to the theoretical value of 1.725 kPa with the error being 1.8%.

It is noted that vocal fold tissues are commonly modeled using transversely isotropic material. While we can use $pR/\Delta x_{\max}$ to evaluate the local stiffness, however, to the best of our knowledge, there is no available analytical solution to verify against. To ensure the accuracy, the in-house finite element solver was extensively validated against the commercial software ABAQUS by comparing the calculation of the cases with transversely isotropic materials. The difference between the in-house finite element solver and the commercial software was within 0.1%.

2.2 Vocal fold model

Figure 1(b) shows the cross-section profile of a simplified vocal fold model. It consists of a rectangular glottal part and a triangular subglottal part. The vocal fold has two layers with the cover layer only present in the medial part and being 0.4 mm thick which was the longitudinal average of the data by Hirano *et al.* (1981). The vocal fold profile was extruded in the longitudinal direction by a length of 15 mm to form the three-dimensional model.

The vocal fold was discretized with ten-node tetrahedral elements. The anterior, posterior, and lateral faces were fixed and the other faces were free surfaces except the indenter boundaries. The indenter boundaries were set in the anterior-posterior middle, and their alignment with respect to the inferior and superior edges is shown in Fig. 1(b). The diameter of the indenter boundary was 1 mm.

To measure the inferior-superior difference in the stiffness, in each case, the inferior aspect and superior aspect were indented, respectively. The vertical stiffness difference (VSD) was calculated as

$$\mathrm{VSD} = \frac{k_{\mathrm{inf}} - k_{\mathrm{sup}}}{k_{\mathrm{sup}}} \times 100\%, \tag{4}$$

where k_{inf} and k_{sup} are the stiffness measured at the inferior and superior aspect, respectively.

The material properties used in this study were adopted from Alipour *et al.* (2000) and are listed in Table 1.

2.3 Variation of material

To model the material stiffness variation, a vertical material difference (VMD) was introduced in the cover layer and was defined as

$$\mathrm{VMD} = \frac{E_{\mathrm{inf}} - E_{\mathrm{sup}}}{E_{\mathrm{sup}}} \times 100\%, \tag{5}$$

where E_{inf} is the elastic modulus at the location of the inferior indenter center and E_{sup} is the elastic modulus at the location of the superior indenter center.

Table 1. Material properties.

Model	Material type	Layer	Young's modulus E_p(kPa)	Longitudinal Young's modulus E_l(kPa)	Longitudinal shear modulus G_l(kPa)	Poisson's ratio[a] μ
1	Isotropic		3.14			0.3
2	Transversely isotropic	cover	2.014	20	10	0.48
		body	3.99	40	12	0.48

[a]For transversely isotropic materials, the Poisson's ratio refers to longitudinal Poisson's ratio.

The following formula was used to specify the location-specific modulus in the cover layer:

$$E(y) = E_0 + E_0 \frac{\text{VMD}}{100} \frac{(y_{\text{sup}} - y_c)}{(y_{\text{sup}} - y_{\text{inf}})}, \tag{6}$$

where $E(y)$ is the local modulus, E_0 is the baseline modulus (values in Table 1), y_c is the vertical coordinate of the geometrical center of the element, y_{sup} and y_{inf} are the vertical position of the center of the superior and inferior indenters, respectively. In this way, the modulus increased linearly (Goodyer *et al.*, 2010) from the superior aspect to the inferior aspect according to the specified VMD. Yang *et al.* (2012) showed that all the stiffnesses (lateral, vertical, and longitudinal) have vertical variation. Thus in the current study, in each case all the three moduli (transverse Young's modulus, longitudinal Young's modulus, and longitudinal shear modulus) were varied simultaneously with the same VMD.

3. Results and discussion

3.1 Effect of subglottal angle

To investigate the effect of subglottal angle, the vocal fold was first modeled using an isotropic material and a one-layer structure. The material properties are shown as model 1 in Table 1. The reason of using the isotropic material and one-layer structure was that the model would be similar to the validation model so that the results can be compared to the analytical solution. The subglottal angle α was changed from 0° to 70° which was about the physiological upper limit (Xu *et al.*, 2017).

The bottom figure of Fig. 2(a) shows the measured stiffness at the inferior and superior aspects of the model with different subglottal angles. The dashed line represents the analytical value. The top figure of Fig. 2(a) shows the calculated VSD at corresponding subglottal angles. It was observed that the VSD increased with the increasing subglottal angle. When the subglottal angle was 0°, the stiffness at the inferior and superior aspects was the same (VSD = 0) due to the inferior-superior symmetry. The stiffness was smaller than the analytical solution, mainly because that the location of the measurement was close to the edge and thus the condition of an infinite half space was not satisfied. As the subglottal angle increased, the stiffness at the inferior aspect increased quickly and saturated beyond the angle of 50°. The saturated value was very close to the analytical solution. This observation suggested that the additional subglottal part provided extra support to the inferior aspect, so that it was more resistant to the loading. The additional subglottal part also extended the edge of the inferior aspect, so that the measurement at the inferior aspect was closer to the condition of an infinite half-space.

The stiffness at the superior aspect also increased with the increasing subglottal angle, but only to a much less extent. It suggested that the additional subglottal support has also stiffened the superior part. However, with a longer distance, the influence was weaker. The VSD basically saturated at the subglottal angle of 40^{0} with a maximum value of about 17%. Therefore, the nonzero subglottal angle of the natural

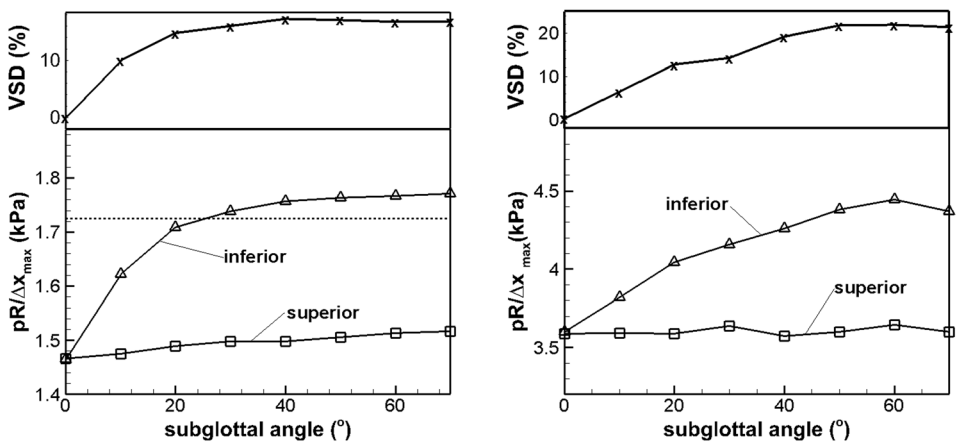

(a) Model 1 in Table 1 (b) Model 2 in Table 1

Fig. 2. The measured stiffness at the inferior and superior aspects of the vocal fold as well as VSD at different subglottal angles for (a) model 1 in Table 1 and (b) model 2 in Table 1. The dashed line in (a) is the analytical value calculated using Eq. (2).

vocal fold shape provides more support for the inferior edge, which increased the stiffness difference between the inferior and superior aspect.

The vocal fold was then modeled using transversely isotropic materials with a body-cover structure. The material properties are shown as model 2 in Table 1. The bottom figure of Fig. 2(b) shows the measured stiffness at the inferior and superior aspects of the model with different subglottal angles. The top figure of Fig. 2(a) shows the calculated VSD at corresponding subglottal angles. The inferior stiffness presented the similar trend as seen in Fig. 2(a) that it increased quickly with the increasing subglottal angle and tended to saturate at the angle of 70°. The superior stiffness, however, presented a different feature that it was nearly unaffected by the subglottal angle. It was unsure whether it was due to the transversely isotropic material or the two-layer structure. VSD increased with the increasing subglottal angle and saturated around the angle of 50° with a maximum value of about 22%. The results indicated that the subglottal angle had similar effects on the transversely isotropic material as on the isotropic material.

3.2 Combined effects of material variation and subglottal angle

As aforementioned, the morphological structure of the vocal fold has already introduced a material stiffness variation in the tissue. It would be of interest to examine the combined effect of the material variation and subglottal angle on the vertical stiffness variation.

A parametric study was performed in a two-dimensional parametric space by varying the VMD from 0 to 90% and the subglottal angle from 0° to 70°. Figure 3 shows the contour of VSD in the parametric space of the subglottal angle and VMD. It is seen that, while the VSD generally increased with the increasing subglottal angle, it showed a tendency of saturation with the increasing subglottal angle. The saturation occurred at larger angles with higher VMD values. For example, at VMD = 0, the saturation occurred at the subglottal angle of about 40°. At VMD around 30%, the saturation occurred at the subglottal angle of about 55°. When VMD was beyond 55%, no saturation was observed up to the subglottal angle of 70°; however, the slowdown of the increase of VSD was observed. Different from the effect of the subglottal angle, the VSD was found to continuously increase with the increasing VMD, and its effect was consistent in the entire range of the subglottal angle. When the subglottal angle was zero, 90% increase in VMD resulted in about 30% increase in VSD. When the subglottal angle was 70°, 90% increase in VMD resulted in about 40% increase in VSD.

Chhetri *et al.* (2014) found an average VMD of about 60% in the measurement of canine samples. Xu *et al.* (2017) reported an average subglottal angle of about 33° during normal phonation based on the models reconstructed from CT (computed tomographic) scans. Assuming the similarities in materials between the human and canine vocal folds, the combination of these two values resulted in a VSD of about 40% based on the data in Fig. 3. This value was in the range of the experimental data on canine vocal folds using micro indentation reported in Oren *et al.* (2014) where the variation ranged from about 16% at 0 strain to about 56% at 0.4 strain. The relatively high value predicted by our model could be due to the uncertainty in material

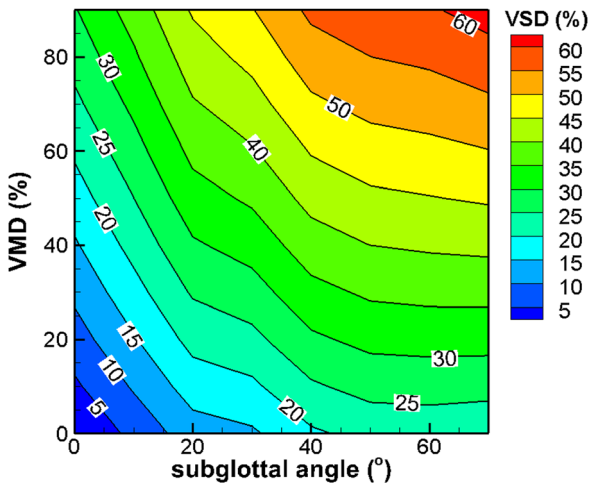

Fig. 3. (Color online) Vertical stiffness difference as a function of VMD and subglottal angle.

properties. The specific value range showed in Fig. 3. should be interpreted with caution since it was associated with the specific material properties and was not generalized. But we expect the general trend should not change for different material properties.

4. Conclusion and implications

A finite element method based numerical indentation technique was used to quantify the contribution of material variation and subglottal angle to VSD. It was found that VSD increased with the increasing subglottal angle, and it tended to saturate beyond a certain subglottal angle. Despite the material stiffness variation, a typical subglottal angle (about 30°–70°, Xu *et al.,* 2017) can cause about 15%–20% differences in the inferior and superior stiffness based on the calculation. This might help explain why in most of the spring-mass models, where the subglottal angle is absent, the lower springs are made stiffer than the upper springs (see, e.g., Ishizaka and Flanagan, 1972; Story and Titze, 1995; Yang *et al.,* 2010). The VSD was also found to continuously increase with the increasing material stiffness variation over the entire range of subglottal angle. The saturation of VSD would occur at larger subglottal angles if the material stiffness variation was increased.

One of the limitations of the current study is that linear elasticity theory was used, so the conclusion might not extrapolate well in the large deformation range. It is unclear how the subglottal angle would interact with highly non-linear material. Besides, the actual inferior-superior stiffness difference is associated with the specific material properties and should be interpreted with caution.

Acknowledgments

The research described was supported by Grant No. 1R03DC014562 from the National Institute on Deafness and Other Communication Disorders (NIDCD). The numerical computation of this study was supported by the Extreme Science and Engineering Discovery Environment (XSEDE) (allocation Award No. TG-BIO150055).

References and links

Alipour, F., Berry, D. A., and Titze, I. R. (**2000**). "A finite-element model of vocal-fold vibration," J. Acoust. Soc. Am. **108**, 3003–3012.

Chhetri, D. K., and Rafizadeh, S. (**2014**). "Young's modulus of canine vocal fold cover layers," J. Voice **28**, 406–410.

Chhetri, D. K., Zhang, Z., and Neubauer, J. (**2011**). "Measurement of Young's modulus of vocal folds by indentation," J. Voice **25**, 1–7.

Geng, B., Xue, Q., and Zheng, X. (**2016**). "The effect of vocal fold vertical stiffness variation on voice production," J. Acoust. Soc. Am. **140**, 2856–2866.

Goodyer, E., Gunderson, M., and Dailey, S. H. (**2010**). "Gradation of stiffness of the mucosa inferior to the vocal fold," J. Voice **24**, 359–362.

Hirano, M., Kurita, S., and Nakashima, T. (**1981**). "The structure of the vocal folds," in *Vocal Fold Physiology*, edited by K. Stevens and M. Hirano (University of Tokyo Press, Tokyo), pp. 33–43.

Ishizaka, K., and Flanagan, J. L. (**1972**). "Synthesis of voiced sounds from a two-mass model of the vocal cords," Bell Syst. Tech. J. **51**, 1233–1268.

Oren, L., Dembinski, D., Gutmark, E., and Khosla, S. (**2014**). "Characterization of the vocal fold vertical stiffness in a canine model," J. Voice **28**, 297–304.

Reidenbach, M. M. (**1996**). "The attachments of the conus elasticus to the laryngeal skeleton: Physiologic and clinical implications," Clin. Anat. **9**, 363–370.

Story, B. H., and Titze, I. R. (**1995**). "Voice simulation with a body-cover model of the vocal folds," J. Acoust. Soc. Am. **97**, 1249–1260.

Xu X., Wang. J., Devine, E. E., Wang. Y., Zhong. H., Courtright, M. R., Zhou. L., Zhuang. P., and Jiang, J. J. (**2017**). "The potential role of subglottal convergence angle and measurement," J. Voice **31**, 116.e1–116.e5.

Yang, A., Berry, D. A., Kaltenbacher, M., and Döllinger, M. (**2012**). "Three-dimensional biomechanical properties of human vocal folds: Parameter optimization of a numerical model to match *in vitro* dynamics," J. Acoust. Soc. Am. **131**, 1378–1390.

Yang, A., Lohscheller, J., Berry, D., Becker, S., Eysholdt, U., Voigt, D., and Döllinger, M. (**2010**). "Biomechanical modeling of the three-dimensional aspects of human vocal fold dynamics," J. Acoust. Soc. Am. **127**, 1014–1031.